Ocean Acoustic Tomography as a Data Assimilation Problem

Pierre Elisseeff and Henrik Schmidt
Department of Ocean Engineering
Massachusetts Institute of Technology
Cambridge, MA 02139

February 18, 1999

Abstract

The Ocean Acoustic Tomographic (OAT) approach to sound speed field estimation is generalized in order to include a variety of sources of information of interest such as an oceanographic model of the sound speed field, direct local sound speed measurements and a full field acoustic propagation model. The inverse problem is presented as a four-dimensional field estimation problem using a variational approach commonly used in oceanographic data assimilation. The OAT approach is shown to be a special case of the general framework. The Matched-Field Tomography (MFT) approach is also discussed within this context. A simple implementation of this novel approach is then investigated in the absence of a suitable oceanographic model. Acoustic propagation is accounted for using a standard parabolic equation model. The inverse equations derived in this paper are validated numerically, and a simple inversion case is discussed.

1 Introduction

Recent advances in sensor technology and computing power have made relatively large data streams of heterogeneous nature available to oceanographers, thus sampling the oceanic environment both locally and remotely. Concurrent advances in acoustical modeling have made it possible to accurately predict acoustic propagation characteristics provided adequate environmental information is available. By combining both data and modeling assets in an operational setting, acoustically focused oceanographic sampling (AFOS) will enable rapid assessment of oceanic fields while drawing on the strength of individual data types, *i.e.*, the large coverage of integral acoustic measurements and the high resolution of local direct measurements [1]. The Haro Strait experiment was implemented in June-July 1996 near Victoria, British Columbia, in order to test a number of engineering and scientific concepts related to coastal oceanic field estimation [2]. The experiment showed that synoptic field estimates can be produced in real time for oceanographically challenging regions, provided that inversion algorithms are kept simple and linear in order to sustain environmental and system uncertainties. It also showed multiple heterogeneous data streams are necessary in order to overcome the inherent limitations of each data type.

While ocean acoustic tomography (OAT) was used for the acoustic measurement model in Haro Strait, it became clear soon after the experiment that the OAT formulation [3] has many limitations preventing it from being an efficient field estimation technique. Drawing on the oceanographic data assimilation literature, the efficient combination of data and models into a field estimate requires three things: a measurement model, capturing the data measurement process; a dynamical model, capturing the deterministic physics of the observed physical process; and a priori statistics for both the data and the model error fields [4]. The OAT approach does provide a priori statistics for the data and the sound speed field. However, it fails to capture the deterministic spatial and temporal physical structure of the sound speed field. Furthermore its associated measurement process is doubly approximate, as it is perturbative and based on a ray-theoretic, partial-wave representation of the acoustic field. In order to palliate these shortcomings and assimilate acoustic data into models, a novel framework has been developed. This framework lays out explicitly a set of four defining equations driven by additive noise terms as outlined in the next section. The resulting sound speed and pressure field estimates agree with both the data and the models within their respective error bounds. The generalized approach represents a first step towards the assimilation of acoustic data into ocean models, and can therefore be referred to as *acoustic data assimilation*.

The example shown in this paper focuses on spatial estimation although time is implicitly taken into account in the formulation. The inversion framework is outlined in the next section. The special cases of OAT and Matched-Field Tomography (MFT) are then investigated. A practical implementation based on the standard parabolic equation model is presented in the following section. Finally, numerical results are shown and discussed in the last section.

2 The Inverse Problem

2.1 General inverse formulation

Information regarding the ocean sound speed field can be drawn from a number of sources when trying to solve the sound speed field inversion problem. Acoustic pressure measurements $\widetilde{\mathbf{p}}$ of the acoustic pressure field $\mathbf{p}$ are gathered by acoustic arrays surrounding the region of interest. Direct (local) measurements $\widetilde{\mathbf{c}}$ of the sound speed field $\mathbf{c}$ might be available, *e.g.*, through CTD data sets. An acoustic wave propagation model $\mathcal{B}$, chosen for its relevance to a particular operational scenario, provides a link between the acoustic measurements and the sound speed field. In addition, further information regarding the spatial and temporal structure of the sound speed field might be contained in what can be loosely called an oceanographic model $\mathcal{A}$. This model may be a simple stochastic constraint or a complex ocean circulation model. These four sources of information are encapsulated in the following set of equations:

$$\widetilde{\mathbf{c}} = \mathbf{M}\mathbf{c} + \mathbf{c}_n, \qquad \mathbf{c}_n \sim N(\mathbf{0}, \mathbf{R}_c) \tag{1}$$

$$\mathcal{A}(\mathbf{c}) = \mathbf{v}, \qquad \mathbf{v} \sim N(\mathbf{0}, \mathbf{Q}_a) \tag{2}$$

$$\mathcal{B}(\mathbf{p}, \mathbf{c}) = \mathbf{w}, \qquad \mathbf{w} \sim N(\mathbf{0}, \mathbf{Q}_b) \tag{3}$$

$$\widetilde{\mathbf{p}} = \mathbf{L}\mathbf{p} + \mathbf{p}_n, \qquad \mathbf{p}_n \sim N(\mathbf{0}, \mathbf{R}_p) \tag{4}$$

The first equation corresponds to the *local sound speed measurement model.* The gaussian noise vector $\mathbf{c}_n$ accounts for local sampling errors. The second equation corresponds to the *oceanographic dynamical model*, thus called by analogy with the oceanographic data assimilation problem. It is driven by the gaussian noise vector $\mathbf{v}$ accounting for unmodeled features of the sound speed field. The third equation corresponds to the *acoustic dynamical model.* It relates the true pressure field to the true sound speed field. It is driven by the gaussian noise vector $\mathbf{w}$ accounting for model uncertainties such as surface roughness, bottom composition, bathymetric uncertainties, sensor locations. The fourth equation corresponds to the *acoustic pressure measurement model.* The additive noise component is here again modeled as a gaussian random vector with known covariance matrix $\mathbf{R}_p$.

The inverse problem now amounts to the estimation of the two state vectors $\mathbf{p}$ and $\mathbf{c}$. Note that the sound speed field $\mathbf{c}$ is understood in general terms; the equations described in this section remain the same regardless of whether $\mathbf{c}$ represents the actual sound speed field, a set of EOF coefficients or any other adequate mapping. Following the traditional variational approach, an optimal estimate of the sound speed field can be computed by minimizing the misfit between the available data sets and the available models, *i.e.*, by jointly minimizing the mean square errors of equations (1)–(4):

$$\widehat{\mathbf{c}} = \underset{p,c}{argmin}\,\{J(\mathbf{p}, \mathbf{c})\} \tag{5}$$

where the objective function J is given by:

$$J(\mathbf{p}, \mathbf{c}) = \mathbf{c}_n^\dagger \mathbf{R}_c^{-1} \mathbf{c}_n + \mathbf{v}^\dagger \mathbf{Q}_a^{-1} \mathbf{v} + \mathbf{w}^\dagger \mathbf{Q}_b^{-1} \mathbf{w} + \mathbf{p}_n^\dagger \mathbf{R}_p^{-1} \mathbf{p}_n \tag{6}$$

Formally minimizing the objective function given above yields:

$$\mathbf{L}^\dagger \mathbf{R}_p^{-1} \mathbf{L}\mathbf{p} + \frac{\partial \mathcal{B}^\dagger}{\partial \mathbf{p}} \mathbf{Q}_b^{-1} \mathcal{B} = \mathbf{L}^\dagger \mathbf{R}_p^{-1} \widetilde{\mathbf{p}} \tag{7}$$

$$\frac{\partial \mathcal{B}^\dagger}{\partial \mathbf{c}} \mathbf{Q}_b^{-1} \mathcal{B} + \frac{\partial \mathcal{A}^\dagger}{\partial \mathbf{c}} \mathbf{Q}_a^{-1} \mathcal{A} + \mathbf{M}^\dagger \mathbf{R}_c^{-1} \mathbf{M}\mathbf{c} = \mathbf{M}^\dagger \mathbf{R}_c^{-1} \widetilde{\mathbf{c}} \tag{8}$$

The system of equations (7)–(8) is coupled through two separate entities. The first is as expected the acoustic model $\mathcal{B}$: it formally relates the acoustic pressure field to the sound speed field. The second entity is the covariance matrix associated with the acoustic dynamical model, *i.e.*, the model error covariance matrix $\mathbf{Q}_b$. If the model error statistics are not quantified the eigenvalues of $\mathbf{Q}_b$ become infinite, thus expressing the fact that no information is available regarding possible model errors. The inverse of $\mathbf{Q}_b$ then tends towards zero and equations (7) and (8) become uncoupled. Equation (7) then reduces to the problem of estimating the acoustic pressure field given the acoustic data only. Equation (8) reduces to the oceanographic data assimilation problem in the absence of acoustic data. In order to preserve the natural coupling exhibited by equations (7) and (8), and therefore optimally estimate the sound speed field using both the available data sets and the available models, error fields must be carefully quantified through the different covariance matrices in general and $\mathbf{Q}_b$ in particular. Solving jointly (7) and (8) will yield an optimal sound speed estimate $\widehat{\mathbf{c}}$ which will agree with all data sets and models available *within their respective error bounds.* In particular this estimate will include the full physics of wave propagation and possibly ocean circulation as specified by (2) and (3). As a byproduct the acoustic field will also be estimated.

An alternate version of the system of equations (7)–(8) can be derived when the acoustic dynamical model $\mathcal{B}(\mathbf{p},\mathbf{c})$ is written as $\mathbf{p}-\mathbf{\Phi}(\mathbf{c})$ and the oceanographic dynamical model $\mathcal{A}(\mathbf{c})$ is written as $\mathbf{c}-\mathbf{\Psi}$:

$$\left(\mathbf{L}^\dagger\mathbf{R}_p^{-1}\mathbf{L}+\mathbf{Q}_b^{-1}\right)\mathbf{p}=\mathbf{L}^\dagger\mathbf{R}_p^{-1}\widetilde{\mathbf{p}}+\mathbf{Q}_b^{-1}\mathbf{\Phi} \tag{9}$$

$$\frac{\partial\mathbf{\Phi}}{\partial\mathbf{c}}\mathbf{Q}_b^{-1}\mathbf{\Phi}+\left(\mathbf{M}^\dagger\mathbf{R}_c^{-1}\mathbf{M}+\mathbf{Q}_a^{-1}\right)\mathbf{c}= \mathbf{M}^\dagger\mathbf{R}_c^{-1}\widetilde{\mathbf{c}}+\mathbf{Q}_a^{-1}\mathbf{\Psi}+\frac{\partial\mathbf{\Phi}}{\partial\mathbf{c}}\mathbf{Q}_b^{-1}\mathbf{p} \tag{10}$$

where $\mathbf{\Phi}$ represents an acoustic propagation model which takes $\mathbf{c}$ as input and returns $\mathbf{p}$ as output; $\mathbf{\Psi}$ represents an oceanographic model whose input is independent of both $\mathbf{p}$ and $\mathbf{c}$ and returns $\mathbf{c}$ as output. This alternate set of equations may be more suitable to some numerical implementations, in particular when derivatives of the acoustic model are available, *e.g.*, through automated differentiation tools such as TAMC [5].

2.2 Simplified inverse formulation

In many cases an oceanographic dynamical model is not available, either because the region of interest is poorly understood, or because such a model is computationally too demanding. Furthermore, direct sound speed measurements might not be included in the inversion, either because they do not exist, or because they are used independently for validation purposes. In this case, which is of practical relevance to many ocean acoustic applications, the original set of equations (1)–(4) becomes:

$$\mathbf{c}-\mathbf{c}_0=\mathbf{c}_n, \qquad \mathbf{c}_n\sim N(\mathbf{0},\mathbf{S}) \tag{11}$$

$$\mathcal{B}(\mathbf{p},\mathbf{c})=\mathbf{w}, \qquad \mathbf{w}\sim N(\mathbf{0},\mathbf{Q}_b) \tag{12}$$

$$\widetilde{\mathbf{p}}=\mathbf{L}\mathbf{p}+\mathbf{p}_n, \qquad \mathbf{p}_n\sim N(\mathbf{0},\mathbf{R}_p) \tag{13}$$

Equation (11) simply expresses the fact that the sound speed field is now modeled as a random vector of known statistics. This is the weakest practical constraint which can be imposed upon $\mathbf{c}$. The objective function becomes:

$$J(\mathbf{p},\mathbf{c})=\mathbf{c}_n^\dagger\mathbf{S}^{-1}\mathbf{c}_n+\mathbf{w}^\dagger\mathbf{Q}_b^{-1}\mathbf{w}+\mathbf{p}_n^\dagger\mathbf{R}_p^{-1}\mathbf{p}_n \tag{14}$$

Minimizing the objective function leads to the following set of equations:

$$\mathbf{L}^\dagger\mathbf{R}_p^{-1}\mathbf{L}\mathbf{p}+\frac{\partial\mathcal{B}^\dagger}{\partial\mathbf{p}}\mathbf{Q}_b^{-1}\mathcal{B}=\mathbf{L}^\dagger\mathbf{R}_p^{-1}\widetilde{\boldsymbol{p}} \tag{15}$$

$$\frac{\partial\mathcal{B}^\dagger}{\partial\mathbf{c}}\mathbf{Q}_b^{-1}\mathcal{B}+\mathbf{S}^{-1}(\mathbf{c}-\mathbf{c}_0)=\mathbf{0} \tag{16}$$

or, alternatively:

$$\left(\mathbf{L}^\dagger\mathbf{R}_p^{-1}\mathbf{L}+\mathbf{Q}_b^{-1}\right)\mathbf{p}=\mathbf{L}^\dagger\mathbf{R}_p^{-1}\widetilde{\mathbf{p}}+\mathbf{Q}_b^{-1}\mathbf{\Phi} \tag{17}$$

$$\frac{\partial\mathbf{\Phi}}{\partial\mathbf{c}}\mathbf{Q}_b^{-1}\mathbf{\Phi}+\mathbf{S}^{-1}(\mathbf{c}-\mathbf{c}_0)=\frac{\partial\mathbf{\Phi}}{\partial\mathbf{c}}\mathbf{Q}_b^{-1}\mathbf{p} \tag{18}$$

This system of equations can be solved by different methods. A simple method, though not necessarily practical in operational settings, is outlined in section 3. A more general method would iterate over (15) and (16): assuming an initial sound speed guess, the acoustic pressure field can be estimated through (15). Then this estimate can be used in (16) in order to estimate the sound speed field. The rate of convergence of this method may be improved by adapting the covariance matrix $\mathbf{Q}_b$ at each step in a way that reflects the relative information contents of the data set and the acoustic model. For instance, the acoustic model is expected to be fairly inaccurate at first. As the system is iterated the initial sound speed guess is refined and the acoustic model uncertainty may be expected to decrease accordingly. However, this procedure requires a formal error model which is beyond the scope of this paper and is still the object of active research.

2.3 Ocean Acoustic Tomography

The ocean acoustic tomographic problem is traditionally formulated in terms very similar to Eq.(11)–(13) although the acoustic dynamical model is in fact implicit and hidden in the acoustic measurement model [3]. It can be formally written as:

$$\mathbf{c}=\mathbf{c}_n, \qquad \mathbf{c}_n\sim N(\mathbf{0},\mathbf{S}) \tag{19}$$

$$\widetilde{\boldsymbol{\tau}}=\mathbf{L}\mathbf{c}+\boldsymbol{\tau}_n, \qquad \boldsymbol{\tau}_n\sim N(\mathbf{0},\mathbf{R}_\tau) \tag{20}$$

where the only state variable is $\mathbf{c}$ and the data $\boldsymbol{\tau}$ usually consists of arrival time perturbations. The objective function now reduces to two terms:

$$J(\mathbf{c})=\mathbf{c}_n^\dagger\mathbf{S}^{-1}\mathbf{c}_n+\boldsymbol{\tau}_n^\dagger\mathbf{R}_\tau^{-1}\boldsymbol{\tau}_n \tag{21}$$

The optimal sound speed estimate is found once again by minimizing J:

$$\widehat{\mathbf{c}}=\left(\mathbf{L}^\dagger\mathbf{R}_\tau^{-1}\mathbf{L}+\mathbf{S}^{-1}\right)^{-1}\mathbf{L}^\dagger\mathbf{R}_\tau^{-1}\widetilde{\boldsymbol{\tau}} \tag{22}$$

This expression has been widely used in OAT inversions, and can also be derived using a bayesian maximum likelyhood approach [3]. A number of important limitations can be found in the OAT approach. The measurement model (20) aggregates a perturbative measurement model with an implicit ray-theoretic dynamical model and is as such doubly approximate. The data used in the inversion excludes significant portions of the actual acoustic data acquired. By contrast equations (1)–(4) or the simpler version (11)–(13) feature an exact acoustic measurement model where the matrix $\mathbf{L}$ simply contains the locations of the acoustic sensors on the computational grid. The data $\widetilde{\mathbf{p}}$ include the full wave acoustic data acquired by the acoustic sensors. Furthermore, the acoustic dynamical model is cast in explicit form and is not limited to

ray models. As such the inverse formulation outlined in 2.1–2.2 can be viewed as a generalization of the OAT framework.

2.4 Matched-Field Tomography

The simplified inverse formulation outlined above can also be used to attempt to describe the Matched-Field Tomography (MFT) approach [6, 7]. The key difference is that the acoustic dynamical model is now assumed to be exact, *i.e.* the covariance matrix $\mathbf{Q}_b$ vanishes. Following the traditional MFT assumptions, the sound speed vector $\mathbf{c}$ is non-random but unknown, which can be expressed by the fact that the inverse covariance matrix $\mathbf{S}^{-1}$ vanishes. Using the alternate representation of $\mathcal{B}$ used in Eq.(9)–(10), which is also commonly used in MFT, the system of equations (11)–(13) then reduces to:

$$\widetilde{\mathbf{p}} = \mathbf{L}\mathbf{\Phi}(\mathbf{c}) + \mathbf{p}_n \tag{23}$$

The objective function J has only one term left:

$$J(\mathbf{c}) = \mathbf{p}_n^\dagger \mathbf{R}_p^{-1} \mathbf{p}_n \tag{24}$$

Defining the scalar product of two vectors as:

$$\langle \mathbf{x} | \mathbf{y} \rangle = \mathbf{x}^\dagger \mathbf{R}_p^{-1} \mathbf{y} \tag{25}$$

the objective function becomes simply equal to $||\mathbf{p}_n||^2$. Using this notation, the optimal sound speed estimate can be written as:

$$\widehat{\mathbf{c}}_{MLM} = \underset{c}{argmin}[||\mathbf{L}\mathbf{\Phi}(\mathbf{c})||^2 - 2Re\left\{\langle \mathbf{L}\mathbf{\Phi}(\mathbf{c}) | \widetilde{\mathbf{p}} \rangle\right\}] \tag{26}$$

By contrast the minimum variance estimate derived in the traditional MFT framework using a linear systems approach can easily be derived using Woodbury's identity as [8]:

$$\widehat{\mathbf{c}}_{MV} = \underset{c}{argmin}[||\mathbf{L}\mathbf{\Phi}(\mathbf{c})||^2 - \frac{1}{1 + ||\mathbf{L}\mathbf{\Phi}(\mathbf{c}_t)||^2} |\langle \mathbf{L}\mathbf{\Phi}(\mathbf{c}) | \mathbf{L}\mathbf{\Phi}(\mathbf{c}_t) \rangle|^2] \tag{27}$$

where $\mathbf{c}_t$ represents the true sound speed field. The first term in (27) is usually interpreted in the beamforming literature as the conventional beamforming output [9]. The second term corresponds to the noise nulling operation. Thus at high signal-to-noise ratios, *i.e.*, for large $||\mathbf{L}\mathbf{\Phi}(\mathbf{c}_t)||$, the nulling term in (27) cancels out the conventional term and the objective function is minimized for $\widehat{\mathbf{c}}_{MV}$ equal to $\mathbf{c}_t$. It is worth noticing the maximum-likelihood estimator (see Eq.(26)) exhibits the same structure, namely a conventional term identical to that in (27) and a nulling term. Although the nulling terms are different, both involve what amounts to a correlation between the data $\widetilde{\mathbf{p}}$ or $\mathbf{L}\mathbf{\Phi}(\mathbf{c}_t)$ and a replica $\mathbf{L}\mathbf{\Phi}(\mathbf{c})$.

3 SPE Inversion

3.1 Standard parabolic equation model

For the purpose of this paper as well as for computational reasons we will restrict ourselves to solving the simplified inversion case (section 2.2). Before the set of equations (15)–(16) can be explicitely solved, an acoustic model $\mathcal{B}$ must be specified. We will use the standard parabolic equation model (SPE) for its relevance to a number of operational situations as well as its numerical tractability. The SPE model can be written as [10]:

$$\mathcal{B}(\mathbf{p}, \boldsymbol{\eta}) = \mathbf{B}(\boldsymbol{\eta})\mathbf{p} - \mathbf{b}_0 = \mathbf{0} \tag{28}$$

where $\mathbf{b}_0$ is initialized using a gaussian starter field. The sound speed vector $\mathbf{c}$ has been replaced by the squared index of refraction $\boldsymbol{\eta}$ whose exact mapping is given below (see equation (34)). The matrix $\mathbf{B}$ is defined on a computational grid of M nodes in depth by N nodes in range as follows:

$$\mathbf{B}(\boldsymbol{\eta}) = \begin{bmatrix} \mathbf{C}_1^1 & \mathbf{O} & \dots & \dots \\ -\mathbf{C}_2^1 & \mathbf{C}_1^2 & \mathbf{O} & \dots \\ \dots & \dots & \dots & \dots \\ \mathbf{O} & \dots & -\mathbf{C}_2^{N-1} & \mathbf{C}_1^N \end{bmatrix} \tag{29}$$

The matrix $\mathbf{C}_1^m$ is defined at the m^{th} range bin as:

$$[\mathbf{C}_1^m]_{jj} = \frac{2ik_0}{\Delta r} - \frac{1}{\Delta z^2} + \frac{1}{2}\eta_{j+(m-1)M}, \quad (j,m) \in [1,M] \times [1,N] \tag{30}$$

$$[\mathbf{C}_1^m]_{j,j\pm1} = \frac{1}{2\Delta z^2}, \quad (j,m) \in [1,M-1] \times [1,N] \tag{31}$$

$$[\mathbf{C}_1^m]_{jl} = 0 \qquad \text{otherwise} \tag{32}$$

The matrix $\mathbf{C}_2^m$ is defined as:

$$\mathbf{C}_2^m = -(\mathbf{C}_1^m)^* \tag{33}$$

where the star denotes complex conjugation. The components $\eta_{j+(m-1)M}$ of the model vector $\boldsymbol{\eta}$ are a monotonic function of the sound speed field:

$$\eta_{j+(m-1)M} = k_0^2 (\frac{c_0^2}{c_{jm}^2} - 1) \tag{34}$$

where c_{jm} is the sound speed at the j^{th} depth bin and m^{th} range bin of the computational grid.

3.2 Inverse equations

Armed with the explicit dynamical model outlined in the previous section, the derivatives of $\mathcal{B}$ with respect to $\mathbf{p}$ and $\boldsymbol{\eta}$ can be derived. The operator $\mathcal{B}$ is recast in a form more suitable to analytical differentiation:

$$\mathcal{B}(\mathbf{p},\boldsymbol{\eta}) = \mathbf{B}_0\mathbf{p} + \frac{1}{2}(\mathbf{I}+\mathbf{J})\mathcal{D}(\mathbf{p})\boldsymbol{\eta} - \mathbf{b}_0 \tag{35}$$

where $\mathbf{I}$ is the identity matrix and $\mathbf{J}$ has its sub-diagonal (corresponding to the η_j's of $\mathbf{C}_2$ in $\mathbf{B}(\boldsymbol{\eta})$) set to 1. The operator $\mathcal{D}$ maps a vector onto a diagonal matrix whose diagonal elements are given by the former. Thus, the derivatives of $\mathcal{B}$ are:

$$\frac{\partial\mathcal{B}(\mathbf{p},\boldsymbol{\eta})}{\partial\mathbf{p}} = \mathbf{B}(\boldsymbol{\eta}) \tag{36}$$

$$\frac{\partial\mathcal{B}(\mathbf{p},\boldsymbol{\eta})}{\partial\boldsymbol{\eta}} = \frac{1}{2}\left(\mathbf{I}+\mathbf{J}\right)\mathcal{D}(\mathbf{p}) \tag{37}$$

We can assume without loss of generality that $\boldsymbol{\eta}$ is zero mean. The system of equations (15)–(16) then becomes:

$$\mathbf{L}^\dagger\mathbf{R}_p^{-1}\mathbf{L}\mathbf{p} + \mathbf{B}(\boldsymbol{\eta})^\dagger\mathbf{Q}_b^{-1}\left(\mathbf{B}(\boldsymbol{\eta})\mathbf{p}-\mathbf{b}_0\right) = \mathbf{L}^\dagger\mathbf{R}_p^{-1}\widetilde{\mathbf{p}} \tag{38}$$

$$\frac{1}{2}\left((\mathbf{I}+\mathbf{J})\mathcal{D}(\mathbf{p})\right)^\dagger\mathbf{Q}_b^{-1}\left(\mathbf{B}(\boldsymbol{\eta})\mathbf{p}-\mathbf{b}_0\right) + \mathbf{S}^{-1}\boldsymbol{\eta} = \mathbf{0} \tag{39}$$

In the absence of a reliable acoustic model, the inverse covariance $\mathbf{Q}_b^{-1}$ tends to zero, and the system of equations (38)–(39) becomes uncoupled. If the acoustic model is infinetely reliable, *i.e.*, the covariance $\mathbf{Q}_b$ tends to zero, the solution to Eq.(38)–(39) becomes independent of the data and is equal to the pressure and sound speed field implicitely assumed in $\mathcal{B}$ within the resolution of the inversion.

3.3 Inverse estimates

The system of equations (38)–(39) can be rewritten as:

$$\mathbf{p} = \left[\mathbf{L}^\dagger\mathbf{R}_p^{-1}\mathbf{L} + \mathbf{B}(\boldsymbol{\eta})^\dagger\mathbf{Q}_b^{-1}\mathbf{B}(\boldsymbol{\eta})\right]^{-1} \left[\mathbf{L}^\dagger\mathbf{R}_p^{-1}\widetilde{\mathbf{p}} + \mathbf{B}(\boldsymbol{\eta})^\dagger\mathbf{Q}_b^{-1}\mathbf{b}_0\right] \tag{40}$$

$$\boldsymbol{\eta} = \left[\mathbf{F}(\mathbf{p})^\dagger\mathbf{Q}_b^{-1}\mathbf{F}(\mathbf{p}) + \mathbf{S}^{-1}\right]^{-1} \mathbf{F}(\mathbf{p})^\dagger\mathbf{Q}_b^{-1}(\mathbf{b}_0 - \mathbf{B}_0\mathbf{p}) \tag{41}$$

$$\mathbf{F}(\mathbf{p}) = \frac{1}{2}\left(\mathbf{I}+\mathbf{J}\right)\mathcal{D}(\mathbf{p}) \tag{42}$$

which may be cast in the following symbolic form:

$$\mathbf{p} = \mathbf{f}(\boldsymbol{\eta}) \tag{43}$$

$$\boldsymbol{\eta} = \mathbf{g}(\mathbf{p}) \tag{44}$$

As alluded to in section 2.2 this system might be best solved by iteration. This would however require an error model for $\mathbf{Q}_b$ which is beyond the scope of this paper. Instead, to demonstrate the feasibility of the inversion we will use the concept of ambiguity surface drawn from the MFP literature [11, 10]. Consider the following cost function ϵ:

$$\epsilon(\boldsymbol{\eta}) = \frac{||\mathbf{g}\left[\mathbf{f}(\boldsymbol{\eta})\right] - \mathbf{T}\boldsymbol{\eta}||}{||\boldsymbol{\eta}||} \tag{45}$$

where $\mathbf{T}$ is the model resolution of the inverse, *i.e.*, the optimal estimate $\widehat{\boldsymbol{\eta}}$ is equal to $\mathbf{T}\boldsymbol{\eta}$. The model resolution captures the fact that even with perfect *a priori* knowledge the true sound speed field can only be recovered within the inherent physical limitations of the observing system. The cost function ϵ will therefore vanish when $\boldsymbol{\eta}$ is equal to the true sound speed field. The cost function might reach a relatively small value for other sound speed fields, thus generating "spurious side lobes" to use MFP terminology. An ambiguity surface can therefore be built by computing ϵ for different values of $\boldsymbol{\eta}$. Alternatively standard multivariate minimization algorithms may be applied to ϵ. The sound speed field estimate will be computed by identifying the absolute minimum of ϵ.

4 Numerical Results

4.1 Framework validation

The size of the vectors used in Eq.(38)–(39) tends to be fairly large and memory-intensive: the size of the pressure field for instance is of order N^2 since it describes a two-dimensional field. The size of matrices such as $\mathbf{B}$ is then of order N^4, where N is the number of grid points in one direction and is typically of the order of 100 and above. The numerical implementation of equations (40) and (41) is therefore non-trivial, and would have been altogether impossible a few years ago due to computational limitations. The purpose of this section is to show that such an implementation is possible today and that sound speed fields can be reasonably estimated using the acoustic data assimilation formulation.

The experimental scenario considered in this paper is shown in Fig.1. The receiver array consists of 33 elements equally spaced spanning the entire water column at a range of 50 km. The source frequency was set to a low value, 5 Hz, in order to decrease the computational load since this paper is concerned solely with demonstrating the numerical feasibility of acoustic data assimilation. The receiver noise covariance matrix $\mathbf{R}_p$ is assumed to be of the form $\sigma_p\mathbf{I}$, where the ambient noise level σ_p is set equal to 70 dB re 1 μPa. The sound speed profile

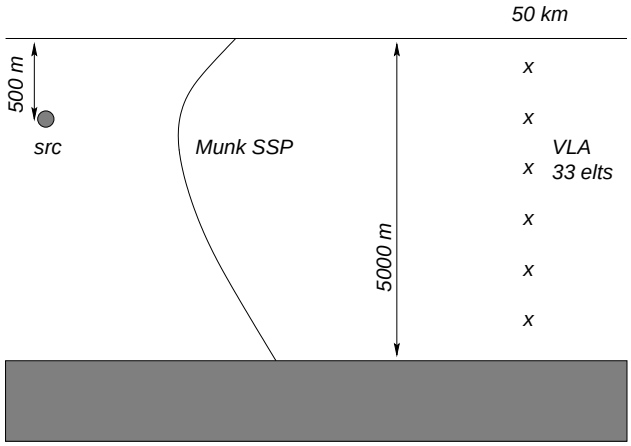

Figure 1: Deep ocean Munk waveguide. Source frequency: 5 Hz. Ambient Noise Level: 70 dB re 1 μPa. Source Level: 190 dB re 1 μPa 1 m.

is a range-independent Munk profile with a channel axis depth of 1300 m (see Fig.4). The sound speed covariance matrix $\mathbf{S}$ is assumed to be of the form $\sigma_s \mathbf{I}$. This covariance matrix really applies to $\boldsymbol{\eta}$, not to the actual sound speed field; the term σ_s was set equal to $2k_0^2$ after calibration of the inversion procedure. Equations (38) and (39) were implemented under the form (43) and (44) using the sparse matrix algebra package UMFPACK [12].

In order to validate the implementation of each equation separately, a pressure field was computed using (43) given the true sound speed field. The result is shown in Fig.2. The reader should bear in mind that this is not an inversion *per se*, but merely the validation of the numerical implementation of $\mathbf{f}(\boldsymbol{\eta})$ in Eq.(43). As expected the field is recovered with a very good accuracy. In order to be consistent with the parabolic equation model presented above, the Hankel function range dependence of the field is not included. The structure of the acoustic model error covariance $\mathbf{Q}_b$ was assumed to be of the form $\sigma_b^2 \mathbf{I}$ where σ_b was set equal to 70 dB re 1 μPa. Conversely, a sound speed field was computed using Eq.(44) assuming the true pressure field was known, and the result is shown in Fig.3 for different values of σ_b. Here again the reader should note this not an inversion *per se*, but the validation of the numerical implementation of $\mathbf{g}(\boldsymbol{\eta})$ in Eq.(44). Note that for the smallest value of σ_b the sound speed field is recovered almost perfectly, except for the region beneath the source, which is not insonified at all and belongs to the null space of the inversion. As the value of σ_b increases, regions that are weakly insonified become impossible to recover.

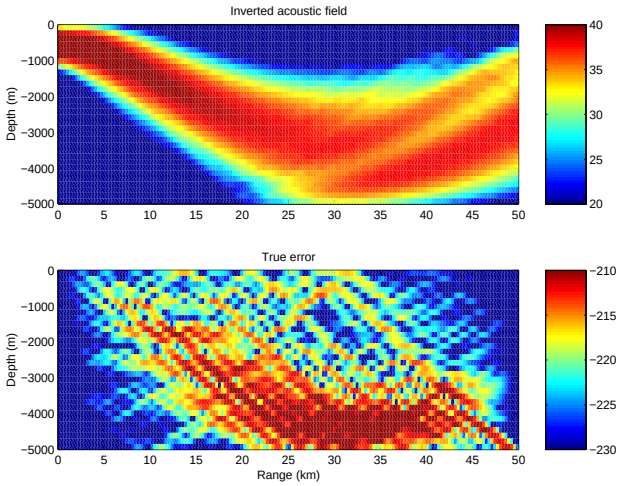

Figure 2: Upper panel: inverted acoustic pressure field when true the sound speed field is known (dB re 1 μPa). Lower panel: true acoustic field error (dB re 1 μPa).

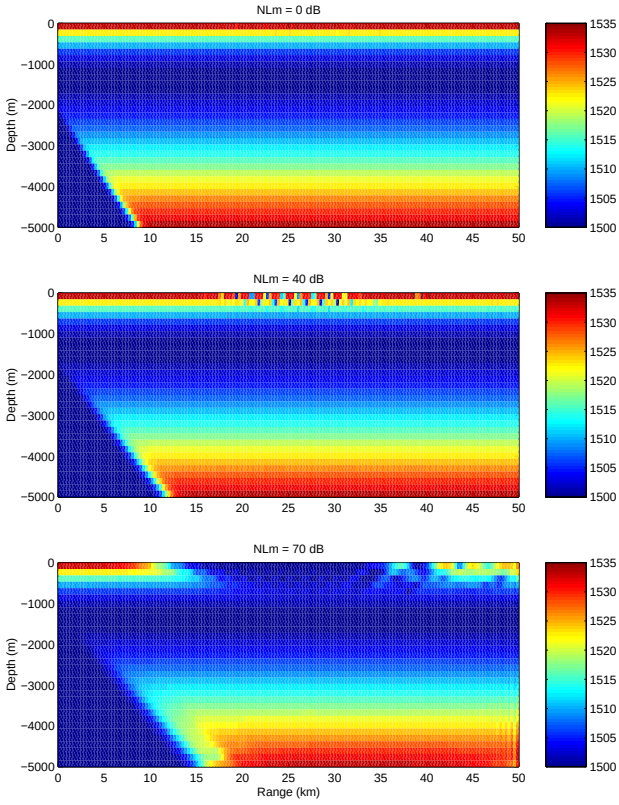

Figure 3: Inverted sound speed field when the true acoustic field is known. Upper panel: the model noise level is 0 dB. Middle panel: the model noise level is 40 dB. Lower panel: the model noise level is 70 dB

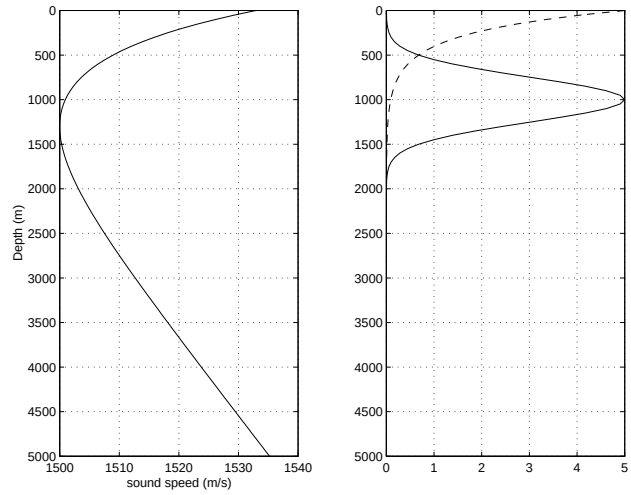

Figure 4: Left panel: climatological (Munk) sound speed profile. Right panel: Empirical orthogonal functions *vs* depth (solid line: EOF1, dashed line: EOF2).

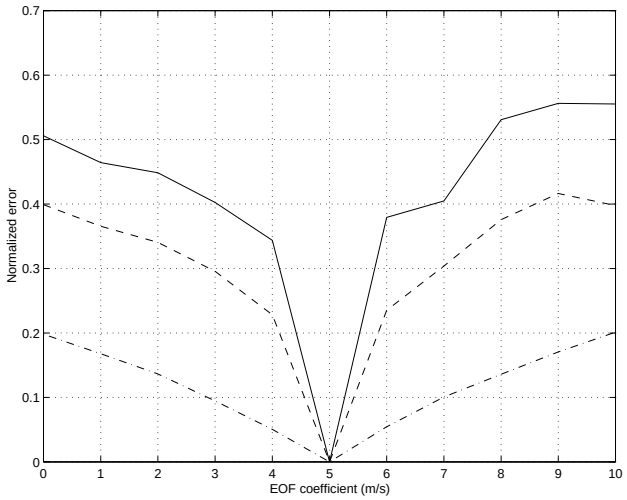

Figure 5: Cost function $\epsilon(\boldsymbol{\eta})$ *vs* EOF1 amplitude for different values of σ_b (solid line: $\sigma_b = 0dB$, dashed line: $\sigma_b = 20dB$, dash-dotted line: $\sigma_b = 40dB$)

4.2 Inversion results

Having validated our numerical implementation in the previous section we can now present a simple inversion scenario in which the true sound speed field is initially unknown and is estimated using the measured acoustic data $\widetilde{\mathbf{p}}$. This scenario assumes an inclusion of warm water is present at a depth of 1000 m. This inclusion is modeled by the empirical orthogonal function (EOF1) shown in Fig.4. Sound speed uncertainties associated with surface temperature changes will be subsequently modeled by the exponentially decaying profile (EOF2) also shown in Fig.4. The resolution matrix $\mathbf{T}$ in Eq.(45)is estimated by computing the inverted sound speed field assuming the true sound speed field is the climatological (Munk) profile. A diagonal pseudo-resolution matrix is then constructed by computing each diagonal element such that the true sound speed field is transformed into its inverse estimate. In the absence of a formal resolution estimate, the resolution matrix is approximated by this pseudo-resolution matrix when computing $\epsilon(\boldsymbol{\eta})$ as defined in Eq.(45).

For the case of no deterministic mismatch, the cost function ϵ is shown in Fig.5 for different amplitudes of EOF1. As the acoustic model noise σ_b decreases, the main lobe of ϵ becomes narrower, indicating that the true magnitude of EOF1 can be identified with a higher accuracy. In other terms the more accurate the acoustic model, the more accurate the sound speed estimate. The same cost function ϵ is next shown in Fig.6 in the presence of a 5 m/s sound speed mismatch at the sea surface, modeled by EOF2. The cost function for σ_b equal to 40 dB is almost the same as in the no mismatch case. The acoustic model is not very accurate, as indicated by the wide main lobe, but it appears to be robust with respect to environmental mismatches. As the model noise decreases, the cost function becomes much more sensitive to environmental mismatch, so that when σ_b is equal to 0 dB, the cost function is no longer well-behaved and a clear minimum is no longer identifiable. In other words, the less accurate the acoustic model, the more robust the sound speed estimate. This outlines the inherent trade-off between accuracy and robustness, which is determined by the choice of σ_b, or more generally $\mathbf{Q}_b$. This trade-off lies at the heart of the inversion methodology presented in this paper: the different sources of noise and error are explicitely accounted for, and presumably quantified through the covariances matrices $\mathbf{Q}_a$, $\mathbf{Q}_b$, $\mathbf{R}_p$ and $\mathbf{R}_c$. Mismatches merely increase the level of uncertainty and may be dealt with provided this increase in uncertainty in properly quantified. Possible biases may be straightforwardly added to the formulation without any significant modification. The price paid for this increased uncertainty will be loss of accuracy or resolution. On the other hand, as the inversion is iterated the covariance matrices may be updated and adapted in order to reflect the actual accuracy of the estimate. The inversion can thus be gradually "focused" in a way similar to that suggested by Collins and Kuperman [13].

In addition, it must be noted that by increasing significantly the level of complexity taken into account in the inversion, the present approach increases by an equal

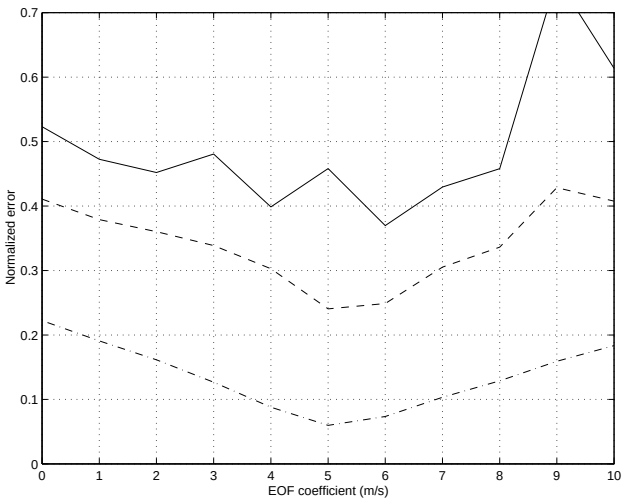

Figure 6: Cost function $\epsilon(\boldsymbol{\eta})$ *vs* EOF1 amplitude for different values of σ_b in the presence of environmental mismatch (solid line: $\sigma_b = 0dB$, dashed line: $\sigma_b = 20dB$, dash-dotted line: $\sigma_b = 40dB$)

amount the computational load required to carry the inversion. Computing Eq.(45) currently takes about 6 to 7 minutes on a Pentium II 450 Mhz running Linux, whereas the signal frequency is only 5 Hz. The focus of this paper however is to show the feasibility of such an approach, and as such does not focus on computational performance issues. Although the available computing power is expected to keep increasing at a rapid pace, this added computational load can already be handled through different numerical and analytical means. Firstly, the present analysis inverts the entire acoustic field whereas only the field in the vicinity of the receiver array is needed for sound speed estimation purposes. Restricting the inverted acoustic field in such a way would reduce the size of the estimated acoustic field by 90%, thus yielding a very significant reduction in the size of a number of matrices involved. In order to do so, the field starter $\mathbf{b}_0$ in Eq.(28) is first propagated through the water column until the vicinity of the receiver array. Thus, it becomes dependent on the sound speed field, and the associated derivative must be included in the analysis. Secondly, the inversion algorithm requires multiple runs of both the acoustic and the oceanographic (whenever available) models. As such it lends itself naturally to a parallel and distributed implementation. In some cases however the acoustic field itself needs to be forecast, *e.g.*, for tactical or environmental reasons. In such cases acoustic data assimilation is at the present time a computational challenge.

5 Summary

The ocean acoustic tomographic approach to sound speed field estimation has been generalized in this paper in order to include a variety of sources of information of interest such as an oceanographic model of the sound speed field, direct local sound speed measurements and an arbitrary acoustic propagation model. This new approach consists of four defining equations:

- a *direct measurement model*, describing the process by which direct, *e.g.*, CTD, measurements are acquired: it relates the directly measured sound speed field to the true sound speed field;
- an *oceanographic model*, imposing a general constraint on the true sound speed field. It may represent the circulation model available for the region of interest;
- an *acoustic propagation model*, relating the true sound speed field to the true acoustic pressure field;
- an *acoustic measurement model*, describing the process by which acoustic measurements are acquired.

A solution to this set of four equations can be computed in a least square sense. The resulting sound speed and pressure field estimates agree with both the data and the models within their respective error bounds. The strengths of this acoustic data assimilation approach are: (i) all dynamical and measurement processes are laid out explicitly and exactly; (ii) any acoustic propagation model may be used; (iii) all error statistics must be explicitly quantified, in particular model error statistics; (iv) full field acoustic data are used. Environmental or system mismatches are quantified through appropriate error statistics, thus affecting the inversion resolution. By contrast, OAT makes a number of implicit assumptions in its measurement model. In particular, it is a partial-wave and perturbative method. More importantly, neither OAT nor MFT quantify the inaccuracies of the underlying acoustic model, thus leading to a heightened sensitivity to mismatch since the corresponding inversion algorithms assume all modeling and system information to be exact. On the other hand, by increasing the complexity and the amount of information taken into account in the inversion, the computational load is significantly increased. However, this increase can be mitigated by the use of sparse matrix algebra as well as parallel and distributed computing techniques.

6 Acknowledgements

Funding was provided by the Office of Naval Research through Grant No. N00014-97-1-1018. The authors

gratefully acknowledge discussions with Dr Pierre Lermusiaux (Harvard University) regarding data assimilation concepts and their application to the tomographic problem described in this paper.

References

[1] H. Schmidt, J.G. Bellingham, and P. Elisseeff. Acoustically Focused Oceanographic Sampling in coastal environments. In E. Pouliquen, A.D. Kirwan, and R.T. Pearson, editors, *Rapid Environmental Assessment*, pages 145–151. Conference Proceedings Series CP-44, SACLANTCEN, 1997.

[2] P. Elisseeff, H. Schmidt, M. Johnson, D. Herold, N.R. Chapman, and M.M. McDonald. Acoustic tomography of a coastal front in Haro Strait, British Columbia. *Journal of the Acoustical Society of America*, 1999. in press.

[3] W. Munk, P. Worcester, and C. Wunsch. *Ocean Acoustic Tomography*. Cambridge University Press, 1995.

[4] A.R. Robinson, P.F.J. Lermusiaux, and N.Q. Sloan. Data Assimilation. In K.H. Brink and A.R. Robinson, editors, *The Sea*, volume 10, pages 541–594. John Wiley and Sons, 1998.

[5] R. Giering and T. Kaminski. Recipes for adjoint code construction. *ACM Trans. Math. Software*, 1998. in press.

[6] A. Tolstoy. *Matched-Field Processing for Underwater Acoustics*. World Scientific, 1993.

[7] A.B. Baggeroer and H. Schmidt. Cramer-Rao bounds for matched-field tomography and ocean acoustic tomography. In *International Conference on Acoustic and Speech Signal Processing*, 1995.

[8] A.P. Sage and J.L. Melsa. *Estimation theory with applications to communications and control*. McGraw-Hill, 1971.

[9] D.H. Johnson and D.E. Dudgeon. *Array signal processing – concepts and techniques*. Prentice-Hall, 1993.

[10] F.B. Jensen, W.A. Kuperman, M.B. Porter, and H. Schmidt. *Computational Ocean Acoustics*. AIP, 1994.

[11] A.B. Baggeroer, W.A. Kuperman, and H. Schmidt. Matched field processing : Source localization in correlated noise as an optimum parameter estimation problem. *Journal of the Acoustical Society of America*, 83(2):571–587, 1988.

[12] T.A. Davis and I.A. Duff. An unsymmetric-pattern multifrontal method for sparse LU factorization. *SIAM Journal on Matrix Analysis and Applications*, 18:140–158, 1997.

[13] M.D. Collins and W.A. Kuperman. Focalization: environmental focusing and source localization. *Journal of the Acoustical Society of America*, 90(3):1410–1422, 1991.